The Astrophysical Journal, 747:64 (16pp), 2012 March 1 doi:10.1088/0004-637X/747/1/64

SUZAKU X-RAY FOLLOW-UP OBSERVATIONS OF SEVEN UNASSOCIATED *FERMI*-LAT GAMMA-RAY SOURCES AT HIGH GALACTIC LATITUDES

Y. Takahashi[1], J. Kataoka[1], T. Nakamori[1], K. Maeda[1], R. Makiya[2], T. Totani[2], C. C. Cheung[3,9], Ł. Stawarz[4,5], L. Guillemot[6], P. C. C. Freire[6], and I. Cognard[7,8]

[1] Research Institute for Science and Engineering, Waseda University, 3-4-1 Okubo, Shinjuku, Tokyo, 169-8555 Japan; s072803523@akane.waseda.jp
[2] Department of Astronomy, School of Science, Kyoto University, Sakyo-ku, Kyoto 606-8502, Japan
[3] Naval Research Laboratory, Washington DC 20375, USA
[4] Department of High Energy Astrophysics, Institute of Space and Astronautical Science (ISAS), Japan Aerospace Exploration Agency (JAXA), 3-1-1 Yoshinodai, Sagamihara 229-8510, Japan
[5] Astronomical Observatory, Jagiellonian University, ul. Orla 171, Kraków 30-244, Poland
[6] Max-Planck-Institut für Radioastronomie, Auf dem Hügel 69, 53121 Bonn, Germany
[7] Laboratoire de Physique et Chimie de l'Environnement, LPCE UMR 6115 CNRS, 45071 Orléans Cedex 02, France
[8] Station de Radioastronomie de Nançay, Observatoire de Paris, CNRS/INSU, 18330 Nançay, France
Received 2011 October 6; accepted 2011 December 20; published 2012 February 14

ABSTRACT

We report on our second-year campaign of X-ray follow-up observations of unidentified *Fermi* Large Area Telescope (LAT) γ-ray sources at high Galactic latitudes ($|b| > 10^{\circ}$) using the X-ray Imaging Spectrometer on board the *Suzaku* X-ray Observatory. In this second year of the project, seven new targets were selected from the First *Fermi*-LAT Catalog, and studied with 20–40 ks effective *Suzaku* exposures. We detected an X-ray point source coincident with the position of the recently discovered millisecond pulsar (MSP) PSR J2302+4442 within the 95% confidence error circle of 1FGL J2302.8+4443. The X-ray spectrum of the detected counterpart was well fit by a blackbody model with temperature of $kT \simeq 0.3$ keV, consistent with an origin of the observed X-ray photons from the surface of a rotating magnetized neutron star. For four other targets that were also recently identified with a normal pulsar (1FGL J0106.7+4853) and MSPs (1FGL J1312.6+0048, J1902.0−5110, and J2043.2+1709), only upper limits in the 0.5–10 keV band were obtained at the flux levels of $\simeq 10^{-14}$ erg cm^{-2} s^{-1}. A weak X-ray source was found in the field of 1FGL J1739.4+8717, but its association with the variable γ-ray emitter could not be confirmed with the available *Suzaku* data alone. For the remaining *Fermi*-LAT object 1FGL J1743.8−7620 no X-ray source was detected within the LAT 95% error ellipse. We briefly discuss the general properties of the observed high Galactic-latitude *Fermi*-LAT objects by comparing their multiwavelength properties with those of known blazars and MSPs.

Key words: galaxies: active – gamma rays: general – pulsars: general – pulsars: individual (PSR J2302+4442) – X-rays: general

Online-only material: color figures

1. INTRODUCTION

Since its successful launch in 2008 June, the Large Area Telescope (LAT) on board the *Fermi Gamma-ray Space Telescope* (Atwood et al. 2009) has enabled many important breakthroughs in the understanding of the origin of high energy γ-ray emissions of various classes of astrophysical objects. The number of detected γ-ray sources increased dramatically, from 271 objects listed in the 3rd EGRET Catalog (3EG; Hartman et al. 1999)[10] to 1873 in the Second *Fermi*-LAT Catalog (2FGL; Abdo et al. 2012). About 800 γ-ray sources included in 2FGL have been identified as blazars (Ackermann et al. 2011), i.e., jetted active galactic nuclei (AGNs) characterized by strong relativistic beaming. Other associations included pulsars (e.g., Abdo et al. 2010d), high-mass X-ray binaries (e.g., Abdo et al. 2009c), radio galaxies (e.g., Abdo et al. 2010i), pulsar wind nebulae (e.g., Abdo et al. 2010h), supernova remnants (e.g., Abdo et al. 2010g), globular clusters (e.g., Abdo et al. 2010l), starburst galaxies (e.g., Abdo et al. 2010f), and distinct objects like the Large Magellanic Cloud (Abdo et al. 2010j). However, no obvious counterparts at longer wavelengths have been found for as much as 38% of the *Fermi*-LAT objects so that several hundreds of GeV sources currently remain *unassociated* with any known astrophysical systems. Fortunately, an improved localization error for the *Fermi*-LAT (typical 95% confidence radii $r_{95} \sim 0.^{\circ}1$–$0.^{\circ}2$, and even $0.^{\circ}005$–$0.^{\circ}01$ for the brightest sources; Abdo et al. 2012), when compared to that of EGRET (typical $r_{95} \simeq 0.^{\circ}4$–$0.^{\circ}7$), allows for much more effective follow-up studies at radio, optical, and X-ray frequencies, which can help to unravel the nature of the unidentified γ-ray emitters.

In this context, X-ray follow-up observations of unidentified *Fermi*-LAT objects are of particular importance, since some classes of astrophysical sources of γ-rays such as AGNs are strong X-ray emitters as well, while the others, like most of γ-ray emitting pulsars, are faint X-ray sources. Note that assuming the keV-to-GeV emission continuum in the form of a broadband power law ($F_{\nu} \propto \nu^{-\alpha_{x\gamma}}$), which could be a relatively good zero-order approximation in the case of blazar sources but not necessarily in the case of other classes of γ-ray emitters, the monochromatic X-ray flux energy density scales as $[\nu F_{\nu}]_{1\,\mathrm{keV}} = (1\,\mathrm{keV}/0.1\,\mathrm{GeV})^{1-\alpha_{x\gamma}} \times [\nu F_{\nu}]_{0.1\,\mathrm{GeV}} \simeq 3 \times 10^{-3} \times [\nu F_{\nu}]_{0.1\,\mathrm{GeV}}$ for a relatively flat spectral index of $\alpha_{x\gamma} \simeq 0.5$. Hence, if an X-ray counterpart of a bright *Fermi*-LAT source is characterized by, e.g., $[\nu F_{\nu}]_{0.1\,\mathrm{GeV}} \simeq 10^{-11}$ erg cm^{-2} s^{-1} and the X-ray-to-γ-

[9] National Research Council Research Associate, resident at Naval Research Laboratory.
[10] See also Casandjian & Grenier (2008) for the revised catalog of EGRET γ-ray sources.

ray power-law emission continuum with the slope $\alpha_{x\gamma} \geqslant 0.5$, such source can be expected to be detectable with modern X-ray instruments such as *Chandra*, *XMM-Newton*, *Swift*, and *Suzaku* within reasonable exposure times. In particular, a point-source search to the level of $[\nu F_\nu]_{1\,\mathrm{keV}} \sim (10^{-14}$ to $10^{-13})$ erg cm^{-2} s^{-1} is easily attainable with the X-ray Imaging Spectrometer (XIS; Koyama et al. 2007) on board *Suzaku* (Mitsuda et al. 2007) with relatively short exposures of few tens of ks (e.g., Akamatsu et al. 2011). In the case of a positive detection, correlated flux changes at X-ray and γ-ray frequencies provide an identification. The lack of correlated variability, or non-detection of an X-ray counterpart, provides only circumstantial evidence regarding the nature of a studied target. Yet in many cases such evidence may be crucial, since the non-detection of an X-ray counterpart despite a long, dedicated observation of a bright *Fermi*-LAT object may disprove a potential association with given classes of astrophysical sources. That is because, as mentioned above, only a few established high-energy emitters are that bright in γ-rays but very faint in X-rays (e.g., Geminga pulsar; see the discussion in Thompson 2004; Matsumoto et al. 2007).

Thus motivated we started a project to investigate the nature of unidentified high Galactic-latitude *Fermi*-LAT objects through deep X-ray follow-up observations with *Suzaku* XIS. The results of the first-year campaign conducted over the span of *Suzaku* AO4 were presented in Maeda et al. (2011). The AO4 program included four steady/weakly variable *Fermi*-LAT sources from the initial *Fermi*-LAT Bright Source List (0FGL; Abdo et al. 2009b) and can be summarized as follows. The X-ray counterpart for one of the brightest unassociated *Fermi*-LAT objects, 1FGL J1231.1−1410 (also detected by EGRET as 3EG J1234−1318 and EGR J1231−1412), was found. The X-ray spectrum of the counterpart was well fit by a blackbody model with a temperature of $kT \simeq 0.16$ keV plus an additional power-law component dominating above 2 keV photon energies. This power-law component was confirmed in subsequent *Swift* and *XMM-Newton* exposures. Considering a recent identification of 1FGL J1231.1−1410 with the millisecond pulsar (MSP) PSR J1231−1411 (Ransom et al. 2011), in Maeda et al. we concluded that the detected thermal X-ray photons originate from the surface of a rotating magnetized neutron star, while the non-thermal X-ray component is most likely produced within the pulsar magnetosphere. In the case of 1FGL J1311.7−3429, two possibly associated X-ray point sources were discovered, one of which is now excluded from the smaller error ellipse of the GeV emitter as cataloged in the 2FGL (Abdo et al. 2012). The identification of the remaining X-ray counterparts with the respective γ-ray objects remains uncertain despite a robust determination of the spectral and variability properties of the X-ray sources. In the case of 1FGL J1333.2+5056, we found several weak X-ray sources within the *Fermi*-LAT error circle and speculated on the AGN nature of the target. Finally, one X-ray point source was detected at the edge of the error ellipse of 1FGL J2017.3+0603. The physical connection was however viewed as unlikely, since the X-ray source did not coincide with the location of the MSP PSR J2017+0603 discovered by the Nançay radio telescope which constituted a more highly probable association with the *Fermi*-LAT object (Cognard et al. 2011). The MSP identification was later indeed confirmed by the detection of the pulsed emission in the *Fermi*-LAT data, with the same period as the radio pulsations.

In this paper, we report the results of our second-year campaign, conducted over the span of *Suzaku* AO5 (2010 April to 2011 March) which included observations of seven *Fermi*-LAT sources located at high Galactic latitudes ($|b| > 10^\circ$). The targets were selected from the First *Fermi*-LAT Catalog of point sources (1FGL; Abdo et al. 2010e) as objects *unidentified* at the time of writing of the *Suzaku* AO5 proposal. Since then however, four of the selected targets have been associated with MSPs: 1FGL J1902.0−5110 with PSR J1902−5105 (F. Camilo et al. 2012, in preparation), 1FGL J2043.2+1709 with PSR J2043+1711 (Guillemot et al. 2012), 1FGL J2302.8+4443 with PSR J2302+4442 (Cognard et al. 2011), and 1FGL J1312.6+0048 with PSR J1312+00 (Abdo et al. 2012). Moreover, 1FGL J0106.7+4853 has very recently been associated with the normal pulsar PSR J0106+4855 (Pletsch et al. 2011). The *XMM-Newton* and *Swift* satellites detected the weak X-ray counterpart of the MSP in 1FGL J2302.8+4443 (Cognard et al. 2011). In the following, our new *Suzaku* observations and data reduction procedure are described in Section 2. The analysis results are given in Section 3, and discussed further in Section 4 in the context of multiwavelength studies of unidentified *Fermi*-LAT objects.

2. *SUZAKU* OBSERVATIONS AND DATA ANALYSIS

2.1. Observations and Data Reduction

We observed seven unidentified *Fermi*-LAT sources with the *Suzaku* XIS. These seven targets were chosen from the 1FGL catalog according to the following selection criteria: (1) no association claimed at the time of the submission of the *Suzaku* proposal, (2) sources located more than $\pm 10^\circ$ away from the Galactic plane, and (3) the detection significance in the LAT γ-ray band (>100 MeV) exceeding 14σ in the 1FGL catalog. The targets thus selected are listed in Table 1 together with the corresponding *Suzaku* observation logs and the 1FGL γ-ray fluxes and photon indices.

The observations were conducted with three XIS detectors and the hard X-ray detector (HXD; Kokubun et al. 2007; Takahashi et al. 2007). The XIS detector is composed of four CCD cameras. One of the four CCD cameras (XIS1) is back-illuminated CCD and the others (XIS0, XIS2, and XIS3) are front-illuminated CCDs. The operation of XIS2 ceased in 2006 November because of the contamination by a leaked charge. Since none of the studied sources have been detected with the HXD, below we describe the analysis of only the XIS data. The XIS was operated in pointing mode and the normal clocking mode, combined with the two editing modes 3×3 and 5×5 for five targets, and only one editing mode 3×3 for 1FGL J2302.8+4443 and 1FGL J1312.6+0048 because of the telemetry limit.

We conducted all the data reduction and analysis with `HEADAS` software version 6.9 and the calibration database (CALDB) released on 2010 July 30. First, we combined the cleaned event data of the two editing modes using `xselect`. Then we removed the data corresponding to the epoch of low-Earth elevation angles (less than 5°), as well periods (and 60 s after) when the *Suzaku* satellite was passing through the South Atlantic Anomaly (SAA). Moreover, we also excluded the data obtained when the *Suzaku* satellite was passing through the low cutoff rigidity (COR) of below 6 GV. Finally we removed hot and flickering pixels using `sisclean` (Day et al. 1998).

2.2. Data Analysis

X-ray images of each target were extracted from the two operating front-illuminated CCDs (XIS0 and XIS3). In the

Table 1
Suzaku Observation Logs and γ-Ray Properties of the Targets

Name	OBS ID	Pointing Direction[a]		Observation	Effective	γ-ray Photon	γ-ray Flux[b]
		R.A. (deg)	Decl. (deg)	Start (UT)	Exposure (ks)	Index[b]	$F_{0.1-100\,\mathrm{GeV}}$ (erg cm^{-2} s^{-1})
1FGL J0106.7+4853	705010010	16.6433	48.9425	2010/07/15 09:53:44	19.7	2.05	2.64×10^{-11}
1FGL J1312.6+0048	705011010	198.1860	0.8370	2011/01/17 04:38:43	17.5	1.99	1.96×10^{-11}
1FGL J1739.4+8717	705012010	264.8730	87.2900	2010/04/26 23:41:56	16.7	2.12	2.92×10^{-11}
1FGL J1743.8−7620	705013010	265.9610	−76.3420	2010/04/14 00:16:05	34.0	2.14	2.83×10^{-11}
1FGL J1902.0−5110	705014010	285.5220	−51.1700	2010/04/13 06:37:43	38.5	2.10	2.46×10^{-11}
1FGL J2043.2+1709	705015010	310.8220	17.1640	2010/05/03 19:23:03	17.7	2.13	3.15×10^{-11}
1FGL J2302.8+4443	705016010	345.7070	44.7230	2010/06/26 05:52:36	35.6	2.04	4.81×10^{-11}

Notes.
[a] The pointing directions are the values of planned target coordinates.
[b] These values are taken from 1FGL catalog (Abdo et al. 2010e).

Table 2
Results of the *Suzaku* Observations of the Selected *Fermi*-LAT Sources

Name		Position	
	Suzaku Detection	R.A. (deg)	Decl. (deg)
1FGL J0106.7+4853	...	...	...
1FGL J1312.6+0048	SUZAKU J1312+0050	198.235(2)	0.835(2)
1FGL J1739.4+8717	Source[a]	...	...
1FGL J1743.8−7620	...	...	...
1FGL J1902.0−5110	...	...	...
1FGL J2043.2+1709	SUZAKU J2043+1710	310.801(2)	17.171(2)
	SUZAKU J2043+1707	310.822(3)	17.133(3)
1FGL J2302.8+4443	PSR J2302+4442	345.695(3)	44.707(2)

Notes. Positions of detected X-ray sources are presented.
[a] We could not determine the exact position of the source because of extended source image (see Section 3.2).

image correction procedure we applied a "non X-ray background" subtraction, an exposure correction, and a vignetting correction (for details, see Maeda et al. 2011). We then combined the images from both CCDs and smoothed the final maps thus obtained using a Gaussian function with $\sigma = 0.'28$. The resulting images are presented and discussed in Section 3. Although all the γ-ray targets were initially selected from the 1FGL catalog, in all the corresponding figures, thick green ellipses denote the more precise 95% position errors from the 2FGL catalog (Abdo et al. 2012) as described in Section 2.1.

For the further analysis, we selected source regions around each detected X-ray source within the 2FGL error ellipses. The radii of the source extraction regions, denoted in the figures below by thin green circles, were set as $1'$, unless otherwise stated. The corresponding background regions with radii of $3'$ were taken from the low count rate area in the same XIS chips (dashed green circles). We set the detection threshold for X-ray sources at 4σ, based on the signal-to-noise ratio defined as a ratio of the excess events above a background to its standard deviation assuming a Poisson distribution. The X-ray source positions and the corresponding errors were estimated by two-dimensional Gaussian fits, as summarized in Table 2.

For the timing analysis, light curves from the front-illuminated (XIS0, XIS3) and back-illuminated (XIS1) CCDs were combined; the corresponding backgrounds were subtracted using `lcmath`. The light curves constructed in this way provide the net-count rates. To quantify possible flux variations, the χ^2 test was applied to each light curve using `lcstats`. For the X-ray spectral analysis, we generated the RMF files for the detector response and the ARF files for the effective area using `xisrmfgen` and `xissimarfgen` (Ishisaki et al. 2007). In order to improve the statistics, we added X-ray counts from the two front-illuminated CCDs, using `mathpha` with no error propagation so that the resulting data follow a Poisson distribution, and then combined the response files using the `marfrmf` and `addrmf` commands. In the case of the γ-ray targets with no detected X-ray counterparts within the 2FGL error ellipses, we calculated 90% confidence level flux upper limits at the positions of the γ-ray emitters assuming an absorbed power-law model. Uncertainties of the model spectral parameters are computed at the 90% confidence levels. The results of the spectral fitting are summarized in Table 3 and discussed below in more detail.

3. RESULTS

In this section, we first present the results of the new *Suzaku* observations in the order of R.A. for the sources for which we detected X-ray counterparts, followed by the analysis results of the remaining targets with no detected X-ray counterparts. All seven targets have also recently been observed by *Swift*, and below we briefly compare the results of the *Suzaku* and *Swift* observations. We search for radio, infrared, and optical counterparts for all the detected X-ray sources using the NRAO VLA Sky Survey (NVSS) catalog (Condon et al. 1998), the Two Micron All Sky Survey (2MASS) point-source catalog (Skrutskie et al. 2006), and the USNO-B1.0 catalog (Monet et al. 2003).

3.1. 1FGL J1312.6+0048

We discovered one X-ray point source inside the 2FGL error ellipse of 1FGL J1312.6+0048, at [R.A., decl.] = [198.°235(2), 0.°835(2)], designated hereafter as Suzaku J1312+0050, with a detection significance of 9σ (total of 178 net source counts from three detectors). The X-ray image of the targeted field is shown in Figure 1. This X-ray source has recently been detected also by *Swift* X-ray Telescope (XRT; Burrows et al. 2005) at [R.A., decl.] = [265.4229, 0.8348] with 90% position error radius $r_{90\%} = 6.''8$. Since the position accuracy of *Swift* XRT[11] ($\sim 5''$) is better than that of *Suzaku* XIS ($\sim 19''$; Uchiyama et al. 2008), we searched for optical and radio counterparts of the X-ray source using the *Swift* position. We found one possibly related optical emitter USNOB 0908-0218088 at about $5''$ away from

[11] See *Swift* Technical Handbook (http://heasarc.nasa.gov/docs/swift/proposals/appendix_f.html)

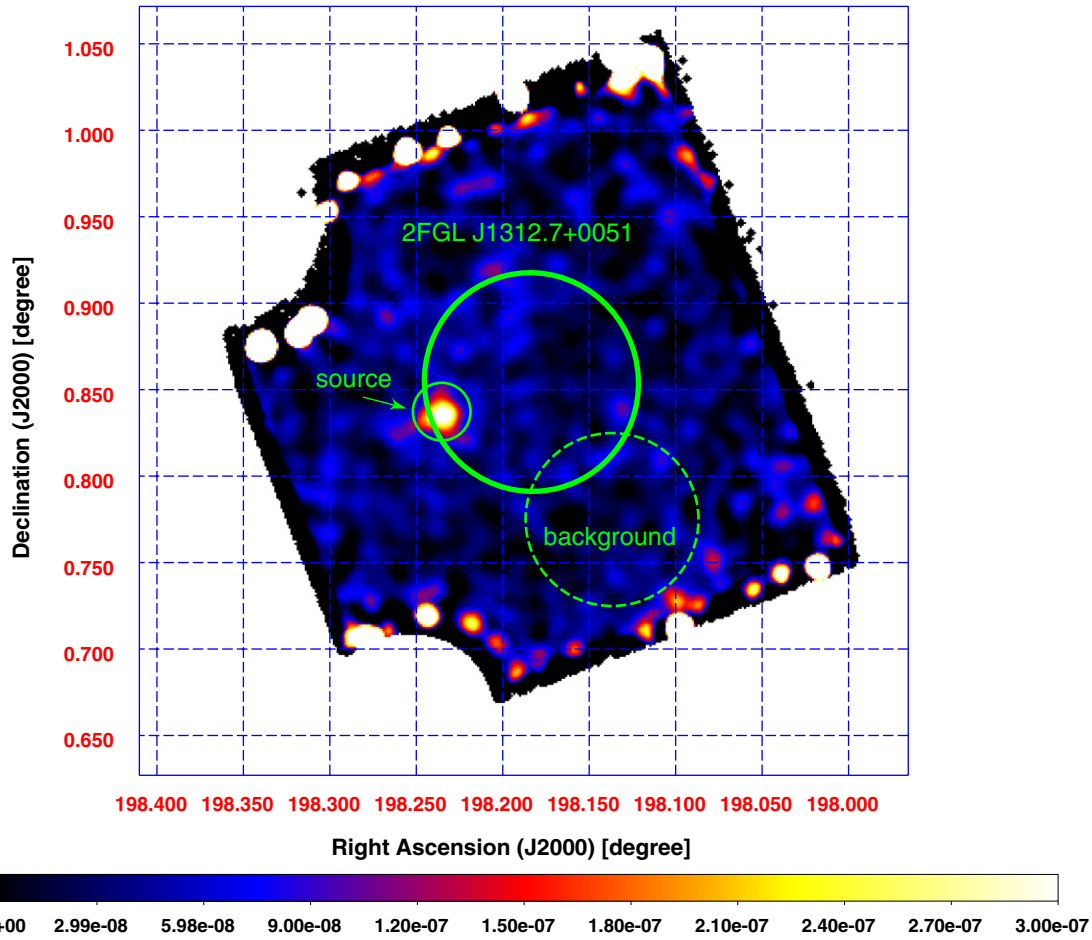

Figure 1. X-ray image of 1FGL J1312.6+0048 by *Suzaku*/XIS0+3 (FI CCDs) in the 0.5–10 keV energy band. Thick solid ellipse denotes the 95% position error of 1FGL J1312.6+0048 in the 2FGL catalog. Thin solid and dashed circles show the source and background regions, respectively. The accurate position of PSR J1312+00 is still not available in the literature.

(A color version of this figure is available in the online journal.)

Table 3
Results of the Analysis of the *Suzaku*/XIS Data and Radio Fluxes of the Sources

Name		$N_{\rm H}$ (10^{20} cm^{-2})	Model	Model Parameter	X-ray Flux $F_{2-10\,\rm keV}$ (erg cm^{-2} s^{-1})	Radio Flux $F_{1.4\,\rm GHz}$ (mJy)
1FGL J0106.7+4853	PSR J0106+4855	11.9 (fixed)	PL	$\Gamma = 2.0$ (fixed)	$<1.0 \times 10^{-14}$	<0.008
1FGL J1312.6+0048	Source	0.0 (fixed)	PL	$\Gamma = 1.9^{+0.4}_{-0.3}$	$8.0^{+2.9}_{-2.6} \times 10^{-14}$	<0.71
	Off-source[a]	2.1 (fixed)	PL	$\Gamma = 2.0$ (fixed)	$<9.3 \times 10^{-14}$	<0.82
1FGL J1739.4+8717	Source	6.36 (fixed)	PL	$\Gamma = 2.1^{+0.5}_{-0.4}$	$3.6\,^{+2.0}_{-1.5} \times 10^{-13}$	<0.58
	NVSS J173722+871744	6.4 (fixed)	PL	$\Gamma = 2.0$ (fixed)	$<1.5 \times 10^{-14}$	61.3
1FGL J1743.8−7620	...	8.13 (fixed)	PL	$\Gamma = 2.0$ (fixed)	$<4.5 \times 10^{-14}$	...
1FGL J1902.0−5110	PSR J1902-5105	4.87 (fixed)	PL	$\Gamma = 2.0$ (fixed)	$<2.5 \times 10^{-14}$	...
1FGL J2043.2+1709	src A	6.63 (fixed)	PL	$\Gamma = 1.67^{+0.16}_{-0.15}$	$2.1^{+0.4}_{-0.4} \times 10^{-13}$	<1.01
	src B	0.0 (fixed)	PL	$\Gamma = 1.6^{+0.4}_{-0.3}$	$9.1^{+3.5}_{-3.0} \times 10^{-14}$	<1.00
	PSR J2043+1711	6.67 (fixed)	PL	$\Gamma = 2.0$ (fixed)	$<3.6 \times 10^{-14}$	0.01[b]
1FGL J2302.8+4443	PSR J2302+4442	0.0 (fixed)	BB	$kT = 0.31^{+0.06}_{-0.05}$ keV	$3.3^{+2.7}_{-2.0} \times 10^{-15}$	1.2[c]

Notes. Summary of analysis results of the seven studied 1FGL sources. Unabsorbed X-ray flux and 90% confidence upper limits in the 2–10 keV band for all the sources are listed. The X-ray upper limits are calculated assuming a power-law model with a photon index of 2 for the 1FGL sources with no X-ray detection. In the seventh column, radio fluxes or upper limits at 1.4 GHz are presented. Radio fluxes and upper limits, the radio values, with no footnote marks were taken either directly from the NVSS (Condon et al. 1998) catalog (for NVSS J173722+871744) or measured by us from the NVSS images (the upper limits; 90% confidence levels).

[a] The evaluated off-source X-ray upper limits expected to represent MSP PSR J1312+00.

[b] This value is estimated by averaging the radio flux over four observations during which the pulsar was detected.

[c] From Cognard et al. (2011).

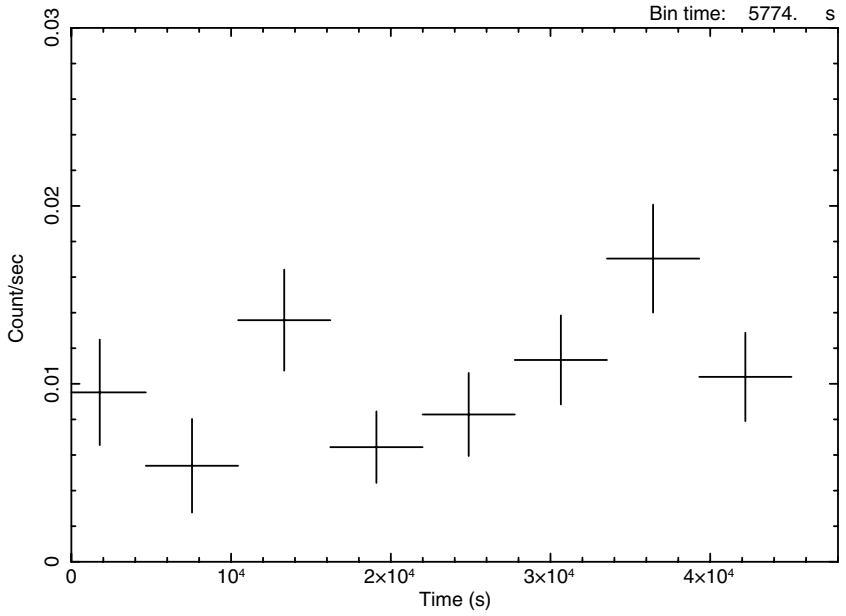

Figure 2. *Suzaku*/XIS light curve of the possible X-ray counterpart of 1FGL J1312.6+0048.

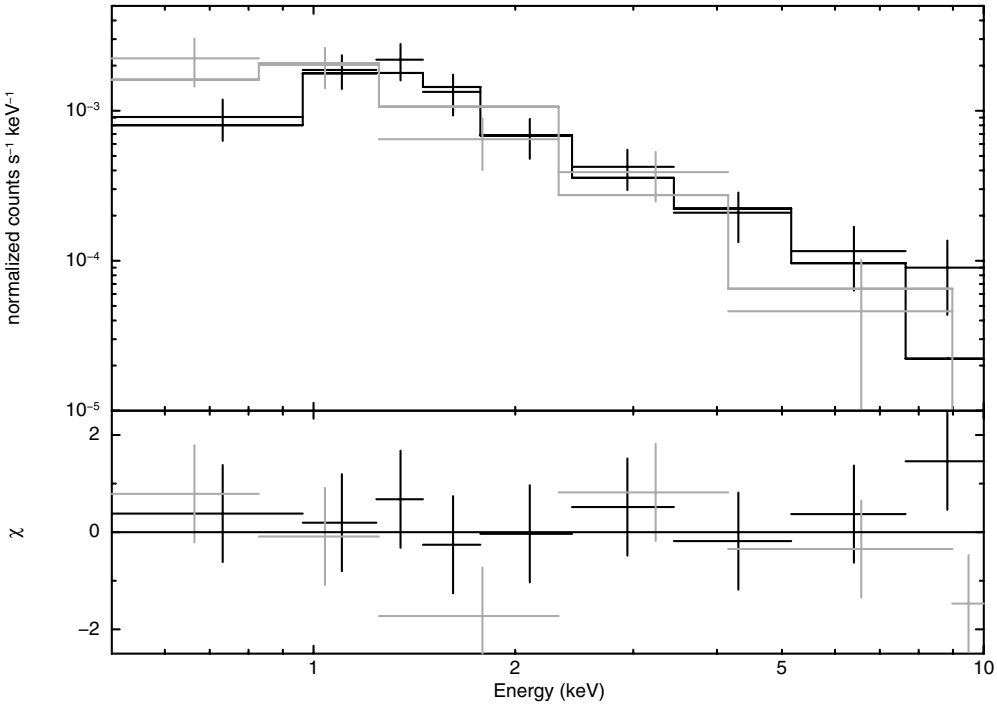

Figure 3. *Suzaku*/XIS spectrum of the possible X-ray counterpart for 1FGL J1312.6+0048 fitted with a power-law model. Black plots show the FI data and gray plots show the BI data.

the X-ray source ([R.A., decl.] = [198.241972(7), 0.83448(5)], and magnitudes B2 = 19.80, R2 = 19.32, and I = 18.11), while no radio and infrared counterparts were discovered.

The light curve of Suzaku J1312+0050 with a time bin of 5774 s and its spectrum are presented in Figures 2 and 3, respectively. The X-ray spectrum when fitted with an absorbed power-law model returned negligible hydrogen column density. We therefore fixed $N_{\rm H} = 0$ and repeated a power-law fit obtaining the photon index of $\Gamma = 1.9^{+0.4}_{-0.3}$ with $\chi^2/{\rm dof} = 9.9/13$. The derived energy flux in the 2–10 keV photon energy range is $8.0^{+2.9}_{-2.6} \times 10^{-14}$ erg cm^{-2} s^{-1}. To test for flux variability, we performed a χ^2 fit with a constant count rate of 1.02×10^{-1} counts s^{-1} resulting in $\chi^2/{\rm dof} = 14.5/7$. This indicates that the X-ray source is variable on the timescale of a few hours, with a probability of $\simeq$96%.

The targeted γ-ray object has recently been associated with the MSP PSR J1312+00 (Abdo et al. 2012). Unfortunately, the position of the radio pulsar is still not available publicly, and hence at this moment we can neither claim nor reject the coincidence of PSR J1312+00 with the detected X-ray source. The variability revealed by the *Suzaku* data, along with the presence of an optical counterpart, implies however that the detected X-ray source is not likely associated with the MSP PSR J1312+00. For this reason we have evaluated the 90% confidence upper limit to the 0.5–2 keV and 2–10 keV fluxes at a random position within the 2FGL error ellipse of

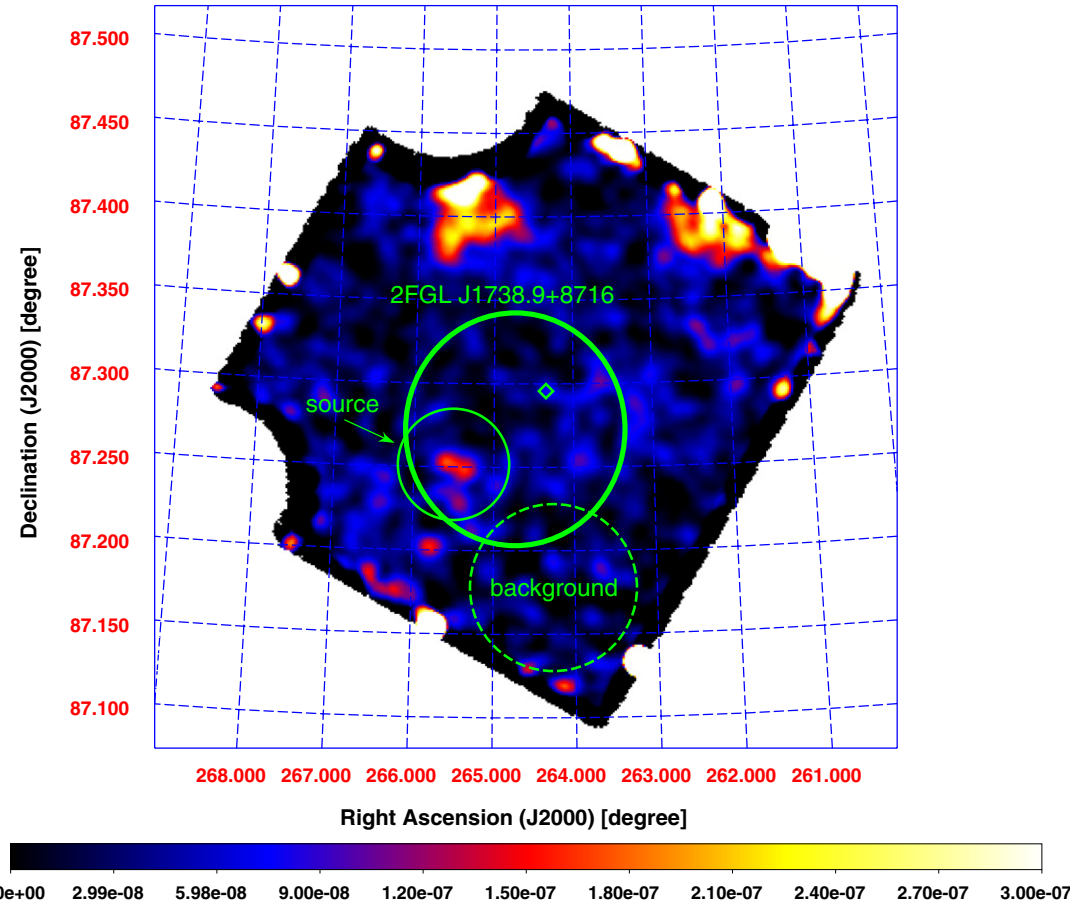

Figure 4. X-ray image of 1FGL J1739.4+8717 by *Suzaku*/XIS0+3 (FI CCDs) in the 0.5–10 keV energy band. Thick solid ellipse denotes the 95% position error of the 2FGL catalog counterpart of 1FGL J1739.4+8717. Thin solid and dashed circles show the source and background regions, respectively. The radio position of NVSS J173722+871744 is marked with a green rhombus.

(A color version of this figure is available in the online journal.)

1FGL J1312.6+0048 (excluding Suzaku J1312+0050), which should correspond (at least roughly) to the upper limits for the X-ray emission of PSR J1312+00. Assuming an absorbed power-law model with $n_{\rm H} = 2.1$ (this value is taken from the LAB Survey of Galactic HI; Kalberla et al. 2005) and photon index $\Gamma = 2$, these read as $<1.3 \times 10^{-13}$ erg cm^{-2} s^{-1} (0.5–2 keV) and $<9.3 \times 10^{-14}$ erg cm^{-2} s^{-1} (2–10 keV), respectively. The implied ratio of the 0.1–100 GeV and 2–10 keV fluxes $F_\gamma / F_{\rm X} > 211$ would then be in agreement with the pulsar association of 1FGL J1312.6+0048 (see Marelli et al. 2011).

3.2. 1FGL J1739.4+8717

As shown in Figure 4, we detected one X-ray source within the 2FGL error ellipse of 1FGL J1739.4+8717 (designated as Suzaku J1742+8715). The detection significance is 7σ (total of 204 net source counts from three detectors). The XIS image of Suzaku J1742+8715 seems to be relatively diffuse. However, *Swift* XRT has recently detected the same X-ray emitter as a point source at [R.A., decl.] = [265.430, 87.245] with 90% position error radius $r_{90\%} = 6\farcs9$. Hence we conclude that in a relatively short *Suzaku* exposure (16.7 ks) the apparently diffuse structure of the object is just an artifact of low photon statistics. We found several weak optical sources coinciding positionally with the X-ray source, but no radio counterpart.

We extracted the source photons from a $2'$ radius circle around Suzaku J1742+8715 and the background photons from a $3'$ radius circle. The resulting X-ray spectrum and X-ray light curve with the time bin of 5760 s are shown in Figures 5 and 6, respectively. A constant fit to the light curve of the X-ray source returned $\chi^2/{\rm dof} = 1.9/6$, indicating that the flux was steady during the *Suzaku* exposure with the χ^2 probability of >93%. The spectrum was initially fitted by an absorbed power-law model ($\chi^2/{\rm dof} = 11.4/12$) and this model returned $N_{\rm H} = 0$. We then refit the spectrum after fixing the $N_{\rm H}$ value to zero and obtained a photon index of $\Gamma = 2.1\pm^{+0.5}_{-0.4}$ and the unabsorbed 2–10 keV flux $3.6^{+2.0}_{-1.5}$ erg cm^{-2} s^{-1}.

We found one relatively bright radio source inside the 2FGL error region of 1FGL J1739.4+8717, namely, NVSS J173722+871744 (∼60 mJy at 1.4 GHz). Its position is marked with a green rhombus in Figure 4. This radio source is detected at several frequencies (151 MHz and 325 MHz; see Baldwin et al. 1985; Rengelink et al. 1997, respectively), but has no obvious X-ray counterpart in our *Suzaku* data. Assuming a power-law form of the radio continuum ($F_\nu \propto \nu^{-\alpha_{\rm r}}$), we calculate the spectral index of NVSS J173722+871744 as $\alpha_{\rm r} = 0.2 \pm 0.1$ from the archival data. This is, in fact, a typical radio spectral index for blazar sources (e.g., Sowards-Emmerd et al. 2005). Moreover, we also found an optical and infrared counterpart, USNOB 1772-0020476 ([R.A., decl.] = [264.35499(2), 87.29532(2)]), which is located only $2\farcs2$ away from the NVSS source with optical magnitudes, B2 = 19.30, R2 = 17.61, and I = 17.07, and 2MASS J17372480+8717433 ([R.A., decl.] = [264.3533(1), 87.2953(1)], and magnitudes $J = 16.2$, $H = 15.5$,

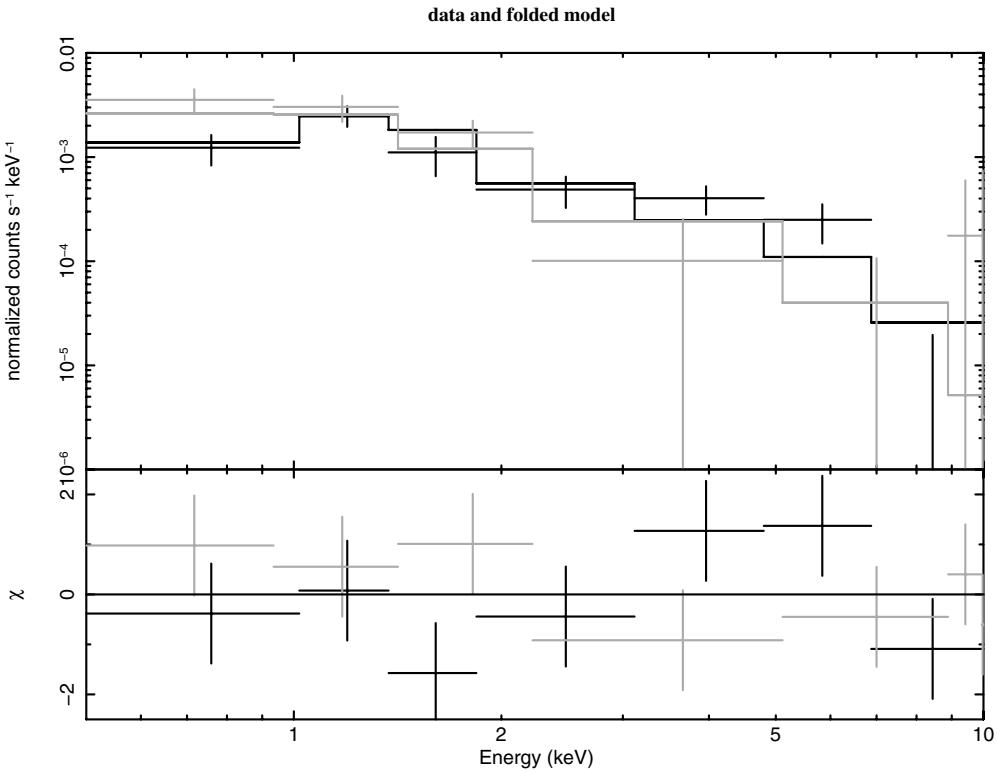

Figure 5. X-ray spectrum of the X-ray counterpart of 1FGL J1739.4+8717 fitted with a power-law model. Black plots show the FI data and gray plots show the BI data.

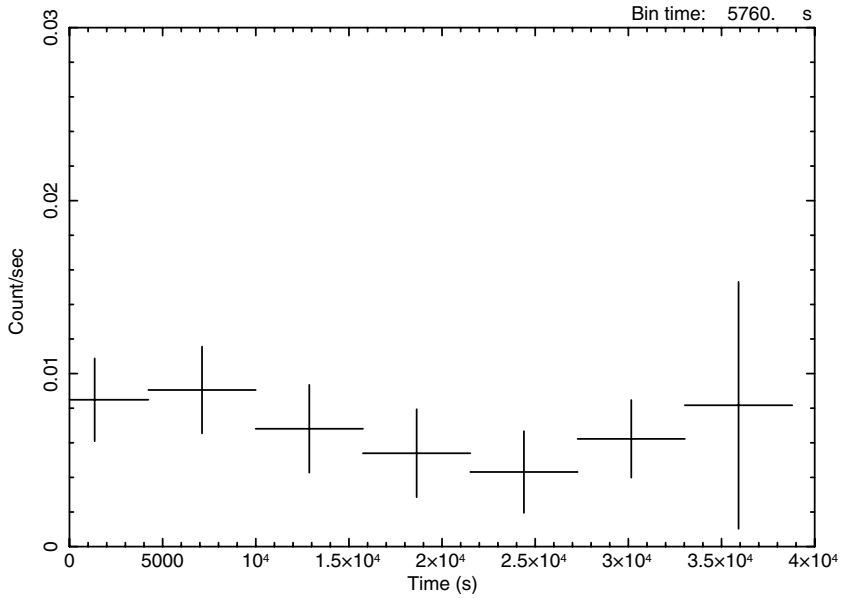

Figure 6. *Suzaku*/XIS light curve of the X-ray counterpart of 1FGL J1739.4+8717.

and $K = 15.8$). This allowed us to calculate radio-to-optical and optical-to-X-ray spectral indices as $\alpha_{ro} = 0.40 \pm 0.01$ and $\alpha_{ox} > 1.77$, with the latter utilizing the X-ray flux upper limit (see Figure 16). These indices are consistent with those of so-called intermediate synchrotron peaked blazars (see Figure 7 in Ackermann et al. 2011).

3.3. 1FGL J2043.2+1709

We found one X-ray point source within the 2FGL error ellipse of 1FGL J2043.2+1709 at the respective position [R.A., decl.] = [310.°801(2), 17.°171(2)], designated as Suzaku J2043+1710, and a second source located on the edge of the ellipse at [R.A., decl.] = [310.°822(3), 17.°133(3)], designated as Suzaku J2043+1707 (hereafter srcA and srcB for short, respectively). These two X-ray objects are not recorded in any available X-ray source catalogs. *Swift* XRT has also detected the same two X-ray emitters. Moreover, *Swift* Ultraviolet/Optical Telescope (UVOT; Roming et al. 2005) discovered a possible UV counterpart of srcA at [R.A., decl.] = [310.80314(6), 17.17286(7)], for which we found an association with the optical source USNOB 1071-0645302 ([R.A., decl.] = [310.80315(7), 17.17300(4)], and magnitudes B2 = 19.89, R2 = 20.6). No radio and infrared counterparts for srcA or srcB were found. The X-ray

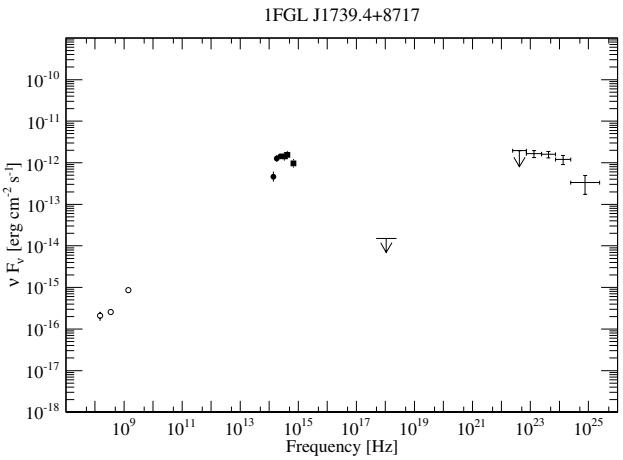

Figure 7. Spectral energy distributions of 1FGL J1739.4+8717. The X-ray data represent 90% confidence upper limit calculated from our *Suzaku* data. The γ-ray data points are taken from the 1FGL catalog (Abdo et al. 2010e). The radio data points are 6C B175708+871924 in 6C catalog (Baldwin et al. 1985), WENSS B1758.4+8718 in WENSS catalog (Rengelink et al. 1997), and NVSS J173722+871744 in NVSS catalog (Condon et al. 1998). Infrared and optical plots, 2MASS J17372480+8717433 and USNOB 1772-0020476, are quoted from 2MASS point source catalog (Skrutskie et al. 2006) and USNO B1.0 catalog (Monet et al. 2003), respectively.

image of the targeted field is shown in Figure 8. The radio position of the MSP PSR J2043+1711 recently associated with the 1FGL J2043.2+1709 is marked in the figure with a green cross centered at [R.A., decl.] = [310.°8370129(2), 17.°1913744(3)].

To extract the spectra and light curves of the detected X-ray sources, we set the source regions and the background region as indicated in Figure 8. The detection significances of both sources were calculated to be 16σ (total of 397 net source counts from three detectors) and 8σ (total of 155 net source counts from three detectors), respectively. No X-ray counterpart of PSR J2043+1711 was detected in our *Suzaku* exposure. The light curves of srcA and srcB with time bins of 5760 s are given in Figure 9, and the corresponding spectra are presented in Figure 10. Both light curves can be well fit by constant count rates (χ^2/dof = 8.5/9 and χ^2/dof = 2.6/9 for srcA and srcB, respectively).

An absorbed power-law model provided the best fit to the spectrum of srcA, returning the photon index $\Gamma = 1.67^{+0.16}_{-0.15}$ and χ^2/dof = 20.4/19. In the fit, the value of $N_{\rm H}$ was frozen at the Galactic value in the direction of the target taken from the LAB Survey of Galactic HI, i.e., 6.63×10^{20} cm^{-2} (Kalberla et al. 2005). We note that the fit with the absorption column density set free returned the value for $N_{\rm H}$ consistent with the Galactic one. The derived unabsorbed X-ray flux of srcA in the

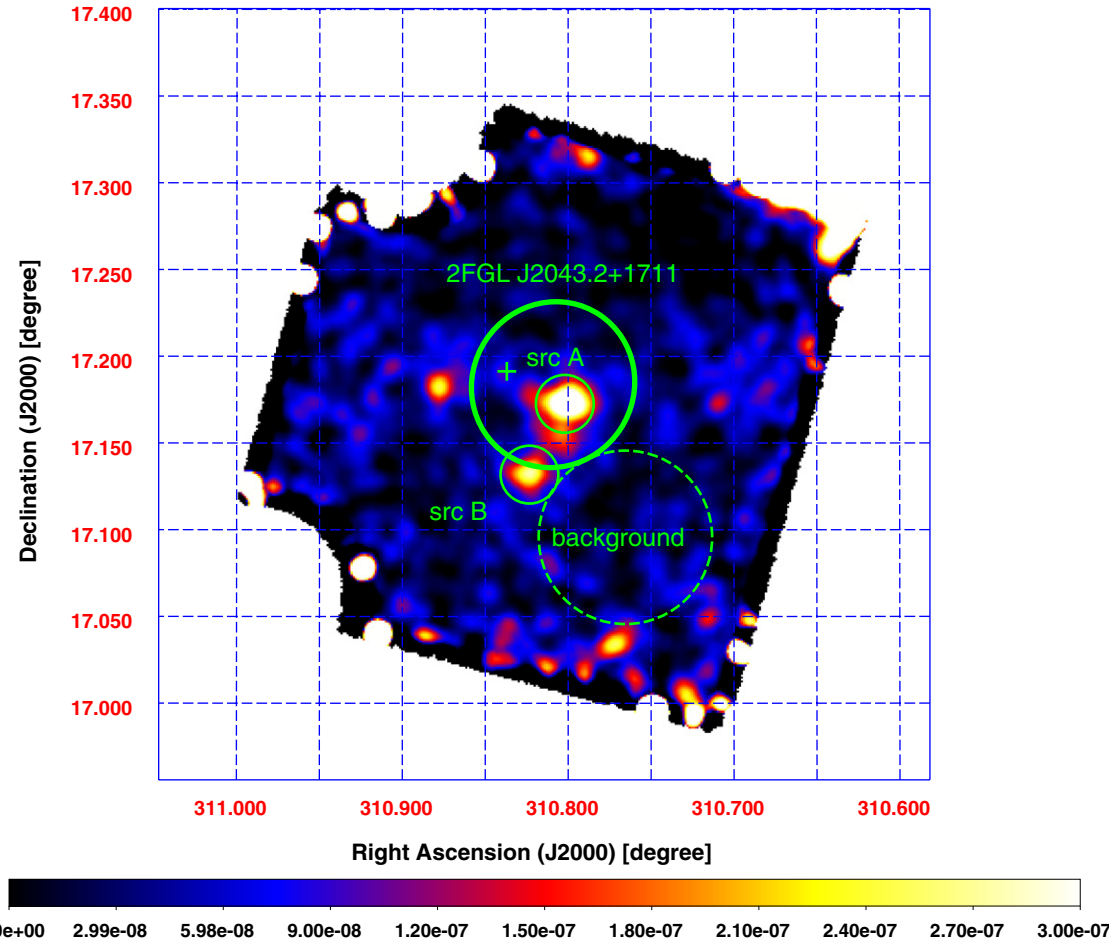

Figure 8. X-ray image of 1FGL J2043.2+1709 by *Suzaku*/XIS0+3 (FI CCDs) in the 0.5–10 keV energy band. The thick solid ellipse denotes the 95% position error of 1FGL J2043.2+1709 from the 2FGL catalog. Thin solid and dashed circles show the source and background regions, respectively. Two X-ray sources inside the positional error ellipse of 1FGL J2043.2+1709 are named srcA for the northern source and srcB for the southern source. The position of the associated MSP PSR J2043+1711 is marked with a cross.

(A color version of this figure is available in the online journal.)

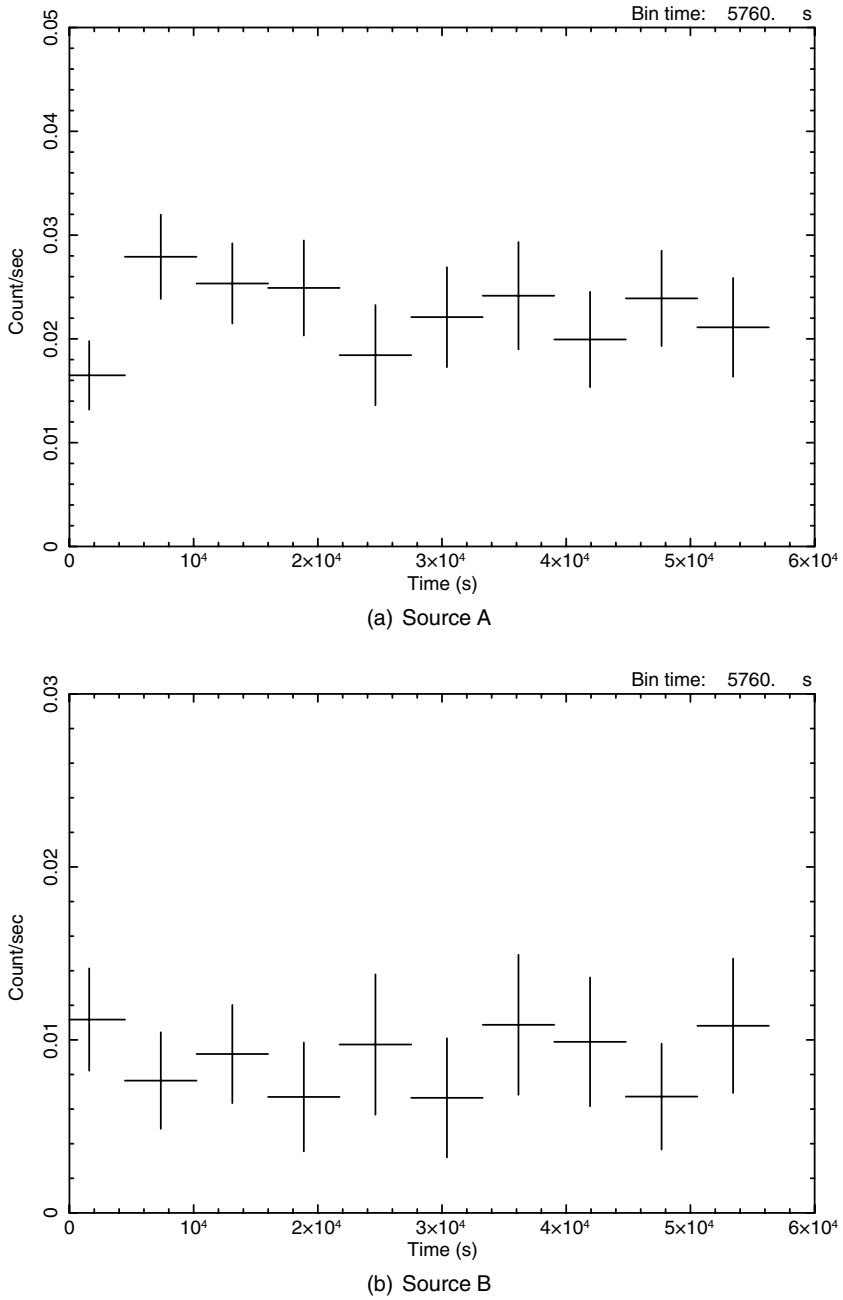

Figure 9. *Suzaku*/XIS light curve of srcA (a) and srcB (b).

2–10 keV photon energy range is $2.1^{+0.4}_{-0.4} \times 10^{-13}$ erg cm^{-2} s^{-1}. Similarly, the X-ray spectrum of srcB was initially fitted with an absorbed power-law model. However, this model fit returned a negligible value of N_H and therefore we fixed $N_{\rm H} = 0$. The best-fit model with χ^2/dof $= 8.6/10$ then returned the photon index $\Gamma = 1.6^{+0.4}_{-0.3}$ and the unabsorbed 2–10 keV flux $9.1^{+3.5}_{-3.0} \times 10^{-14}$ erg cm^{-2} s^{-1}.

Assuming a power-law model with photon index $\Gamma = 2$, we calculated upper limits (90% confidence) in the 0.5–2 keV and 2–10 keV bands at the position of PSR J2043+1711 as $<2.4 \times 10^{-14}$ erg cm^{-2} s^{-1} and $<3.6 \times 10^{-14}$ erg cm^{-2} s^{-1}, respectively. This gives the ratio of the 0.1–100 GeV and 2–10 keV fluxes $F_\gamma/F_{\rm X} > 864$ which is consistent with the values claimed for the GeV-detected MSP (Marelli et al. 2011).

3.4. 1FGL J2302.8+4443

One X-ray point source was discovered inside the 2FGL error ellipse of 1FGL J2302.8+4443 at the position of [R.A., decl.] = [345.°695(3), 44.°707(2)] (designated as Suzaku J2302+4442). The detection significance of this X-ray source was calculated as 5.35σ (total of 121 net source counts from three detectors). As shown in Figure 11, the detected X-ray source coincides with the radio position of the MSP PSR J2302+4442 (green cross centered at [R.A., decl.] = [345.°695748(3), 44.°706136(1)]). This MSP was recently claimed to be associated with 1FGL J2302.8+4443. No optical and infrared counterparts of the pulsar were found. In the analysis of the *Suzaku* data, the source and the background regions were set as indicated in the figure. The light curve of the X-ray counterpart with the time bin of 11520 s is presented in Figure 12. The applied

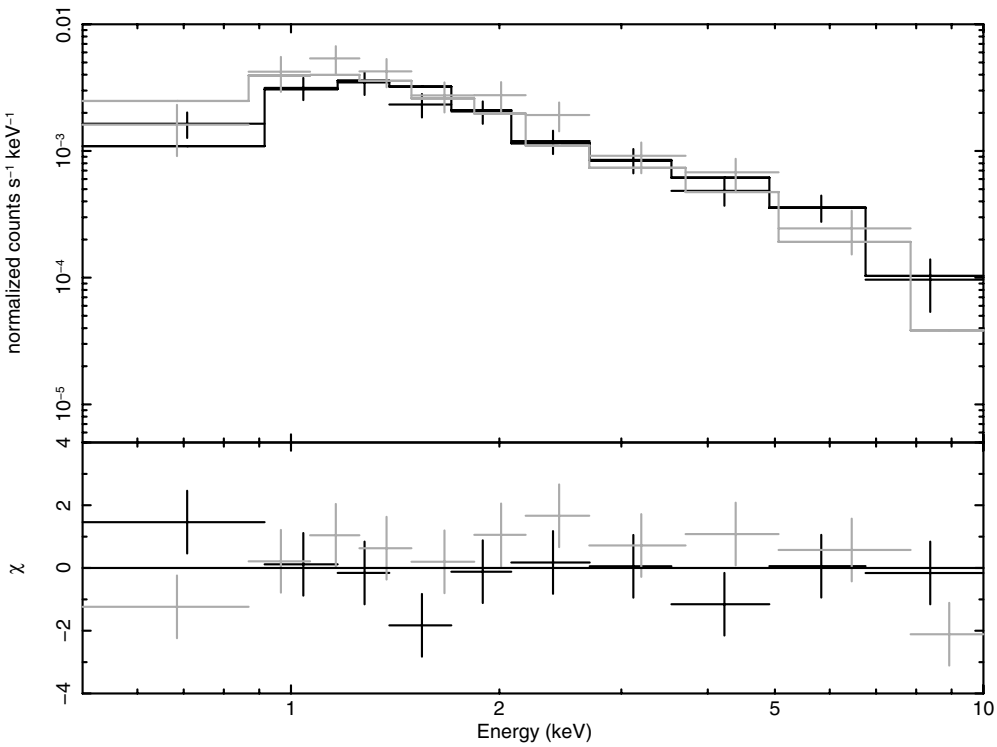

(a) Source A

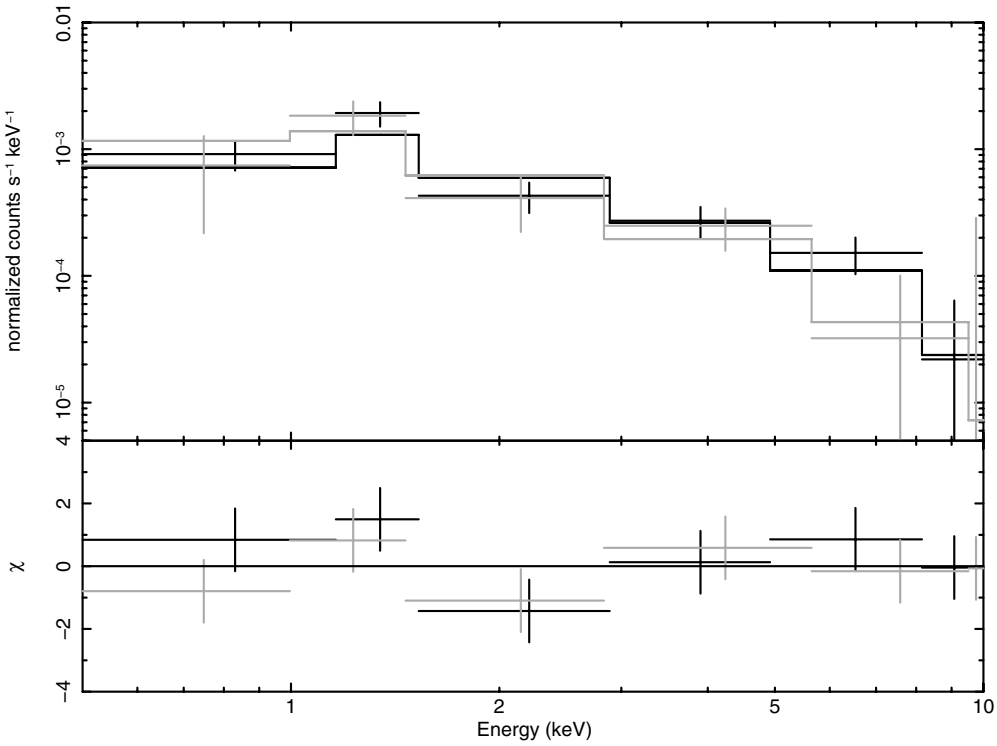

(b) Source B

Figure 10. *Suzaku*/XIS spectra of srcA (a) and srcB (b) inside the error ellipse of 1FGL J2043.2+1709. Both spectra are fitted with an absorbed power-law model. Black plots show the FI data and gray plots show the BI data.

χ^2 test assuming a constant count rate gave $\chi^2/\mathrm{dof} = 4.98/5$, indicating that the X-ray flux was steady during the *Suzaku* exposure.

The XIS spectrum of the detected X-ray source is shown in Figure 13. Initially, we fitted the spectrum with an absorbed power-law model. This model returned an extremely soft

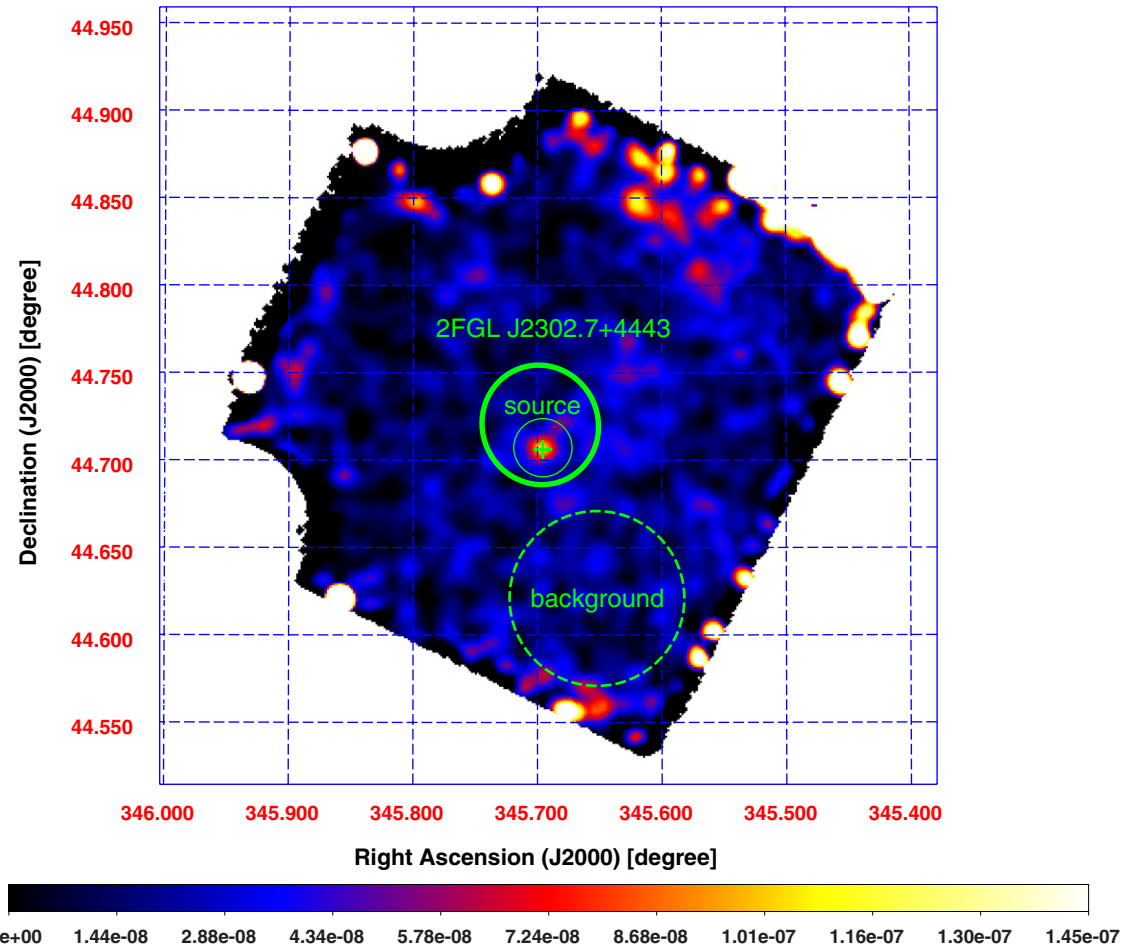

Figure 11. X-ray image of 1FGL J2302.8+4443 by *Suzaku*/XIS0+3 (FI CCDs) in the 0.5–2 keV energy band. Thick solid ellipse denotes 95% position error of 1FGL J2302.8+4443 from the 2FGL catalog. Thin solid and dashed circles show the source and background regions, respectively. The position of the associated MSP PSR J2302+4442 is marked with a cross.

(A color version of this figure is available in the online journal.)

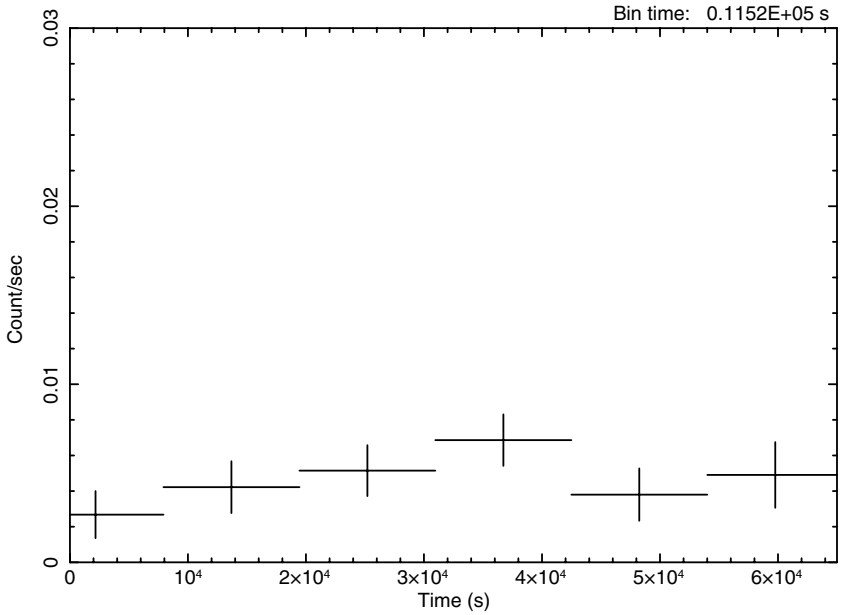

Figure 12. *Suzaku*/XIS light curve of the X-ray counterpart of 1FGL J2302.8+4443.

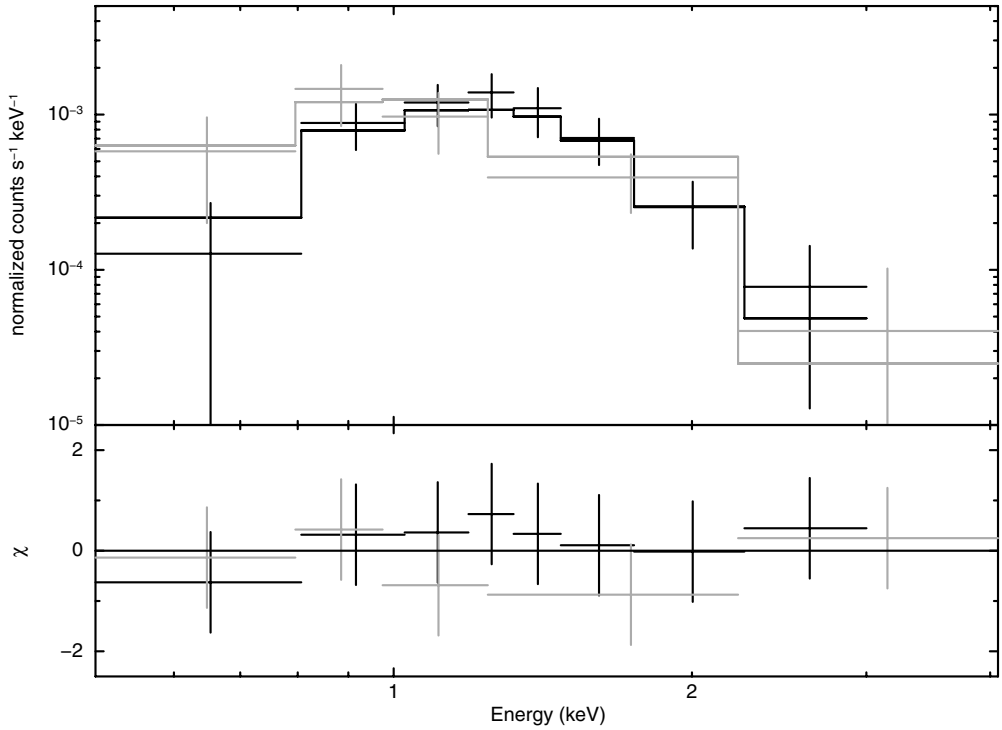

Figure 13. *Suzaku*/XIS spectrum of the X-ray counterpart of 1FGL J2302.8+4443 fitted with a black body model. Black plots show the FI data and gray plots show the BI data.

continuum characterized by a photon index of $\Gamma = 4.5^{+2.1}_{-1.7}$, and a rather high value of $N_{\rm H} = 0.56^{+0.68}_{-0.34} \times 10^{22}$ cm^{-2}. This absorption value is in excess of the Galactic column density in the direction of the target, namely, 0.132×10^{22} cm^{-2}, as determined by Kalberla et al. (2005) from the LAB survey of Galactic HI. Next we applied an absorbed blackbody model but the model fit returned $N_{\rm H}$ consistent with zero. We therefore fixed $N_{\rm H} = 0$ and obtained the best-fit (χ^2/dof = 3.0/11) temperature of $kT \simeq 0.31^{+0.06}_{-0.05}$ keV (see Figure 13). The observed X-ray flux of the source is $2.6^{+0.6}_{-0.5} \times 10^{-14}$ erg cm^{-2} s^{-1} in the 0.5–2 keV range and $3.3\ ^{+2.7}_{-2.0} \times 10^{-15}$ erg cm^{-2} s^{-1} in the 2–10 keV range. The ratio between γ-ray and 2–10 keV fluxes for 1FGL J2302.8+4443/Suzaku J2302+4442 reads as $F_\gamma/F_{\rm X} = 14531$. This ratio is relatively high but still consistent with those of *Fermi*-LAT/LAT pulsars reported in Marelli et al. (2011).

3.5. Other Sources

No X-ray sources were detected in our *Suzaku* exposures inside the 2FGL error ellipses of the remaining γ-ray objects: 1FGL J0106.7+4853, 1FGL J1743.8−7620, and 1FGL J1902.0−5110. The corresponding X-ray images of the targets are shown in Figures 14–16. Out of these three sources, 1FGL J1902.0−5110 has been recently associated with the MSP PSR J1902−5105. Even more recently, after the submission of this paper, 1FGL J0106.7+4853 has also been identified with a new γ-ray pulsar, PSR J0106+4855 (Pletsch et al. 2011). Thus only 1FGL J1743.8−7620 remains at the moment unassociated. We calculated an X-ray upper limit in the 2–10 keV band for the latter source assuming X-ray emission from a point source located at the center of 2FGL error region, obtaining in this way the energy flux $<4.5 \times 10^{-14}$ erg cm^{-2} s^{-1}. In the case of 1FGL J1902.0−5110, we set the X-ray extraction region as a 1′ radius circle around the radio position of PSR J1902−5105. The resulting X-ray upper limits are calculated as $<2.0 \times 10^{-14}$ erg cm^{-2} s^{-1} (0.5–2 keV) and $<2.5 \times 10^{-14}$ erg cm^{-2} s^{-1} (2–10 keV) by assuming an absorbed power-law model with photon index $\Gamma = 2$. Finally, X-ray upper limits for 1FGL J0106.7+4853 were calculated for a circular extraction region with radius 1′ around the position of PSR J0106+4855, obtaining $<7.7 \times 10^{-15}$ erg cm^{-2} s^{-1} (0.5–2 keV) and $<1.0 \times 10^{-14}$ erg cm^{-2} s^{-1} (2–10 keV). For these two pulsars, the ratio of the 0.1–100 GeV and 2–10 keV fluxes are $F_\gamma/F_{\rm X} > 976$ and $F_\gamma/F_{\rm X} > 2640$, respectively. These flux ratios are consistent with the ratios of *Fermi*-LAT pulsars reported in Marelli et al. (2011). The results of the *Swift* observations of all of the three targeted γ-ray emitters are consistent with the *Suzaku* results.

4. DISCUSSION AND CONCLUSIONS

In this paper, we report on the results of X-ray follow-up observations of seven bright *Fermi*-LAT sources at high Galactic latitudes ($|b| > 10^\circ$) using *Suzaku* XIS. We discovered the X-ray counterpart of 1FGL J2302.8+4443 coinciding with the position of the MSP PSR J2302+4442 recently claimed to be associated with the γ-ray emitter. We did not however detect X-ray counterparts for the other four *Fermi*-LAT objects similarly identified with a normal pulsar (1FGL J0106.7+4853) and MSPs, namely 1FGL J1312.6+0048, 1FGL J1902.0−5110, and 1FGL J2043.2+1709. (In a few cases the X-ray sources have been detected within the 2FGL error ellipses, but none at the positions of the pulsars.) A relatively weak X-ray source was found inside the 2FGL error region of 1FGL J1739.4+8717. Finally, no candidate for the X-ray counterpart was detected for the remaining object 1FGL J1743.8−7620.

Including our previous observations of 1FGL J1231.1−1410, 1FGL J1311.7−3429, 1FGL J1333.2+5056, and 1FGL J2017.3+0603 reported in Maeda et al. (2011), our sample of high Galactic-latitude *Fermi*-LAT objects initially selected as

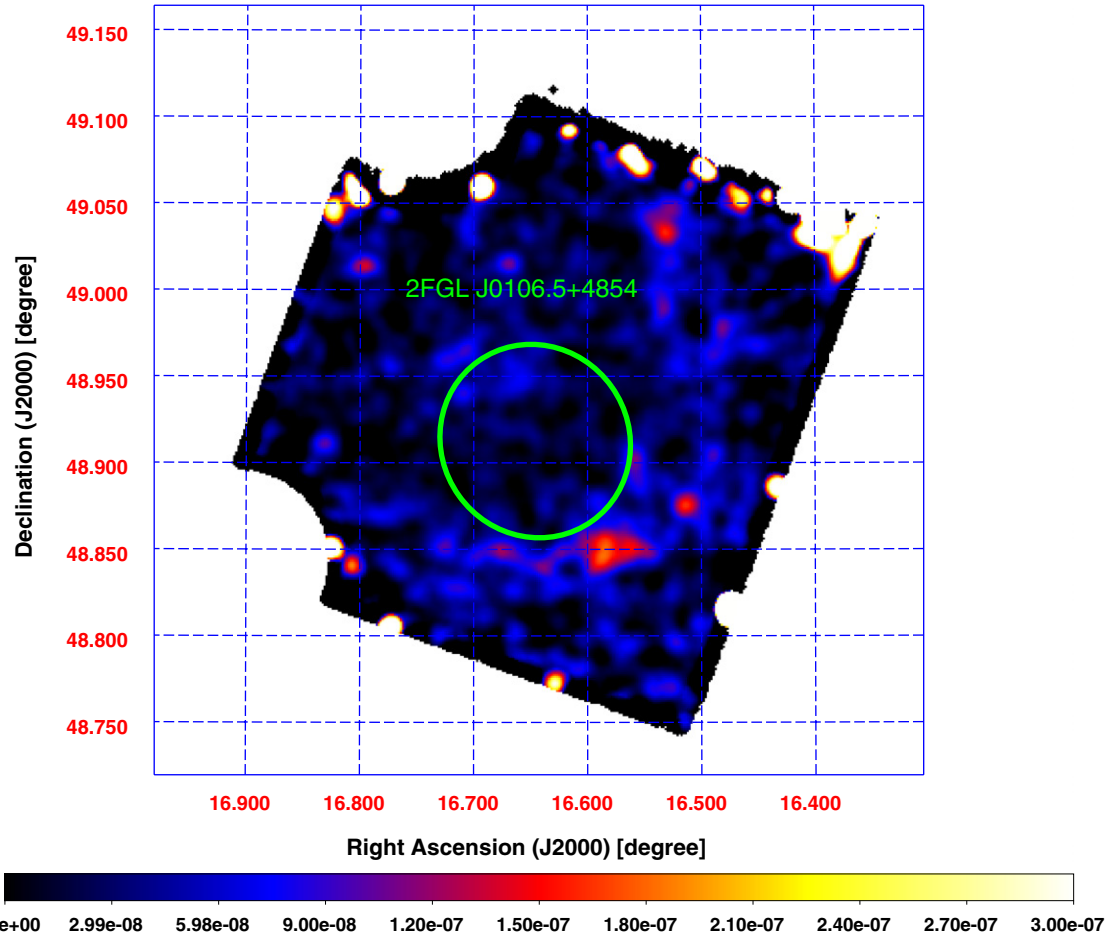

Figure 14. X-ray image of 1FGL J0106.7+4853 by *Suzaku*/XIS0+3 (FI CCDs) in the 0.5–10 keV energy band. Thick solid ellipse denotes 95% position error of 1FGL J0106.7+4853 from the 2FGL catalog.

(A color version of this figure is available in the online journal.)

unidentified and studied with *Suzaku* now consists of 11 targets. For eight of these, we have detected single or multiple X-ray sources within the LAT error ellipses. Over the time period when the *Suzaku* observations were being obtained, six targets from the γ-ray sample were found to be associated with MSPs, one target (1FGL J0106.7+4853) has been associated with a normal pulsar, and one source (1FGL J1333.2+5056) has been classified as an AGN candidate, all in agreement with the gathered X-ray data. Still, four objects from the list remain unidentified. As argued below, one of these four, 1FGL J1739.4+8717, is quite likely a high-redshift blazar.

The source 1FGL J1739.4+8717 was characterized by an enhanced flux level within the LAT photon energy range during the first seven months of *Fermi*-LAT operation.[12] After that time, the activity of the γ-ray emitter decreased. The photon index in the LAT energy band is $\Gamma_\gamma = 2.1 \pm 0.1$ (where $dN/dE \propto E^{-\Gamma_\gamma}$ is the differential photon flux; Abdo et al. 2012), which is a typical value for the γ-ray spectra of BL Lac type blazars (see Ackermann et al. 2011). Importantly, as written in Section 3.2, one relatively bright radio source, NVSS J173722+871744, is located inside the 2FGL error region of 1FGL J1739.4+8717 (see Figure 4). With a typical radio spectral index for blazar sources and radio-to-optical and optical-to-X-ray spectral indices that are consistent with blazar broadband spectrum, it is quite likely that 1FGL J1739.4+8717 is indeed associated with a distant blazar currently characterized by an activity level low enough so that its X-ray emission was below the detection limit of the XIS instrument ($\sim 10^{-15}$ erg cm^{-2} s^{-1}) at the time the *Suzaku* observations were performed.

In general, unidentified sources constituted a large fraction of the population of γ-ray emitters detected by EGRET ($\sim$60% in 3EG), and at present about 31% of *Fermi*-LAT sources in 2FGL catalog remain unassociated (specifically, 273 sources at high Galactic latitudes ($|b| > 10^\circ$) and 303 sources at low Galactic latitudes $|b| < 10^\circ$). Those located at the lowest Galactic latitudes ($|b| < 5^\circ$) are most widely expected to be associated with local systems such as molecular clouds, supernova remnants, massive stars, high-mass X-ray binaries, radio quiet pulsars, and pulsar wind nebulae (e.g., Kaaret & Cottam 1996; Yadigaroglu & Romani 1997; Romero et al. 1999). In particular, half a dozen of the brightest 3EG sources in the Galactic plane were identified as young pulsars (Thompson et al. 1999), despite the relatively poor localization of the EGRET sources and the source confusion complicated substantially the identification procedure. On the other hand, most of the unassociated 3EG sources at high Galactic latitudes ($|b| > 10^\circ$) were later identified as blazars (Sowards-Emmerd et al. 2003, 2004). Pulsars were therefore expected to be found mainly among GeV emitters at low Galactic latitudes, while blazars

[12] http://heasarc.gsfc.nasa.gov/FTP/fermi/data/lat/catalogs/source/lightcurves/2FGLJ1738.9+8716.png

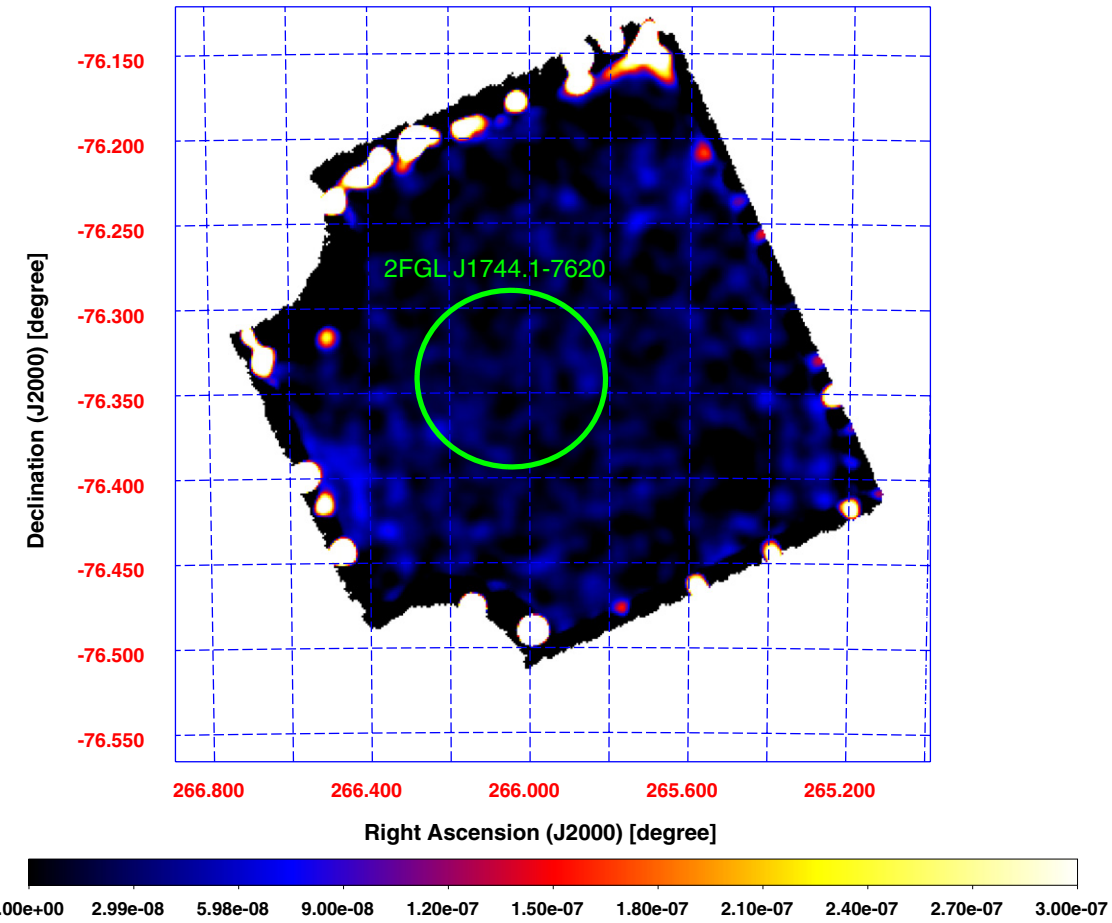

Figure 15. X-ray image of 1FGL J1743.8−7620 by *Suzaku*/XIS0+3 (FI CCDs) in the 0.5–10 keV energy band. Thick solid ellipse denotes 95% position error of 1FGL J1743.8−7620 from the 2FGL catalog.

(A color version of this figure is available in the online journal.)

were supposed to constitute the main population of GeV emitters at high Galactic latitudes. But the γ-ray–bright pulsars were also expected to be found at intermediate Galactic latitudes ($5^\circ < |b| < 73^\circ$; Crawford et al. 2006). The identification of a number of *Fermi*-LAT objects located above the Galactic plane ($|b| > 10^\circ$) with such systems (predominantly with MSPs) confirmed these expectations (see, e.g., Ransom & Pulsar Search Consortium 2010 and the discussion in Maeda et al. 2011).

In Figure 17 we plot the X-ray-to-γ-ray energy flux density ratios ($F_{2-10\,\mathrm{keV}}/F_{0.1-100\,\mathrm{GeV}}$) versus radio-to-$\gamma$-ray energy flux density ratios ($F_{1.4\,\mathrm{GHz}}/F_{0.1-100\,\mathrm{GeV}}$) for the *Fermi*-LAT objects from our *Suzaku* sample discussed here (blue circles) with the radio data available in the literature (Abdo et al. 2010e; Condon et al. 1998, see Table 3). These can be compared with the analogous ratios evaluated for bright *Fermi*-LAT objects identified with blazars and MSPs (denoted in the figure by red crosses and squares, respectively). We remind the reader that the blazar class includes flat spectrum radio quasars (FSRQs) and BL Lacertae objects (BL Lacs). In addition, in the figure we plot the two targets discussed in Maeda et al. (2011), namely, 1FGL J1333.2+5056 most likely associated with an AGN and a peculiar object 1FGL J1311.7−3429 (pink stars). As shown, the blazar and MSP populations are clearly separated in the constructed flux ratio plane. Also, four objects from our sample that have recently been associated with a normal pulsar (1FGL J0106.7+4853) and MSPs (1FGL J1312.6+0048, 1FGL J2043.2+1709, and 1FGL J2302.8+4443) occupy the same region in the analyzed parameter space as the previously known MSPs detected in the GeV range.[13] On the other hand, in the case of 1FGL J1739.4+8717 the evaluated energy flux density ratios—which are very similar to those characterizing 1FGL J1333.2+5056—are consistent with the blazar identification proposed above, if only NVSS J173722+871744 is considered as the true counterpart of the γ-ray emitter.

In all, we conclude that the gathered *Suzaku* XIS data together with the broadband properties of the analyzed *Fermi*-LAT objects are in agreement with the identification of most of them as MSPs. However, a few cases in the analyzed sample (1FGL J1739.4+8717, 1FGL J1333.2+5056) constitute quite probable associations with AGNs (high-redshift blazars). Finally, the nature of the remaining few targets (like 1FGL J1311.7−3429) is still an open question, although, as inferred from Figure 17, the MSP identification seems more viable than the blazar one. In the near future, we are further continuing our X-ray studies during the *Suzaku* AO6 cycle, focusing on both new targets (1FGL J0103.1+4840, 1FGL J1946.7−5404, and 1FGL J2339.7−0531), but also performing ultradeep exposures on particularly intriguing sources like 1FGL J1311.7-3429.

[13] In the case of 1FGL J1312.6+0048, the X-ray-to-γ-ray energy flux density ratio shown in Figure 17 is evaluated assuming the association of the γ-ray sources with the MSP PSR J1312+00. That is, the *Suzaku* XIS upper limit derived at the position of the pulsar is considered, and not the X-ray flux of the *Suzaku* source detected within 2FGL error region.

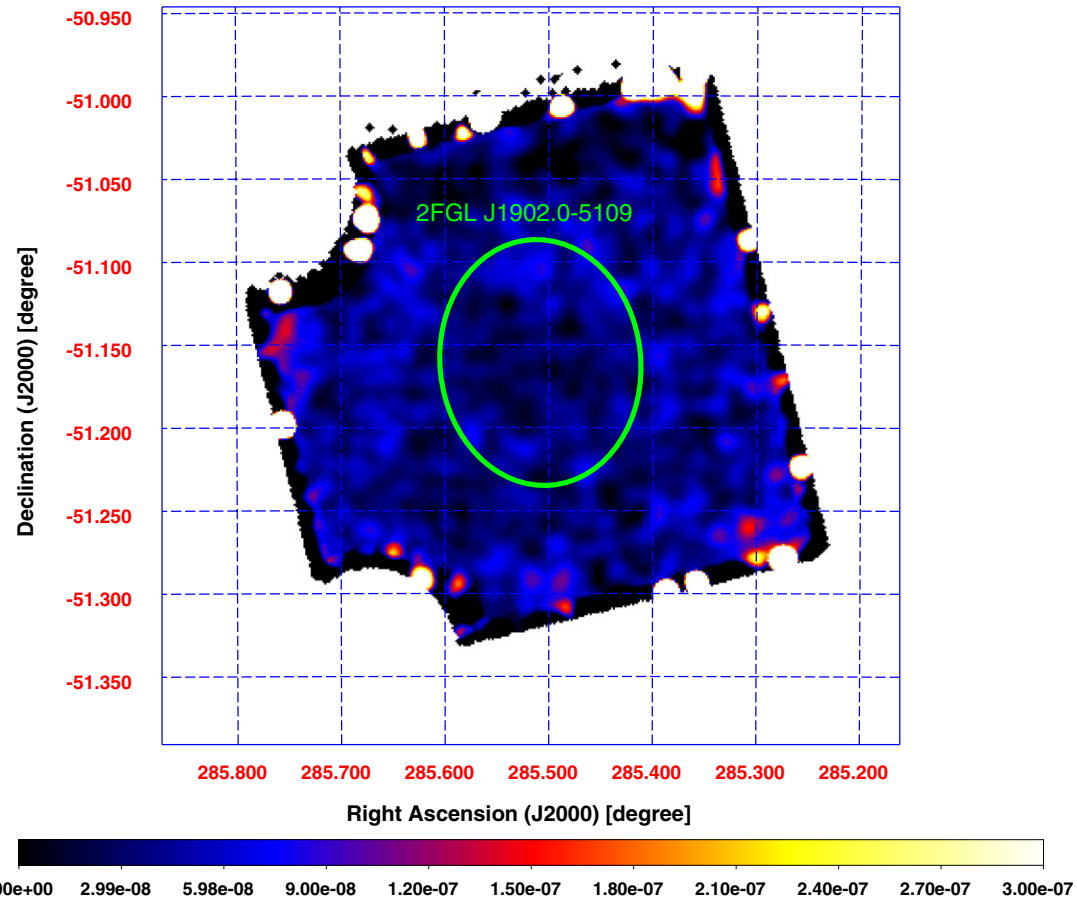

Figure 16. X-ray image of 1FGL J1902.0−5110 by *Suzaku*/XIS0+3 (FI CCDs) in the 0.5–10 keV energy band. Thick solid ellipse denotes 95% position error of 1FGL J1902.0−5110 from the 2FGL catalog. The accurate position of PSR J1902−5105 is still not available in the literature.

(A color version of this figure is available in the online journal.)

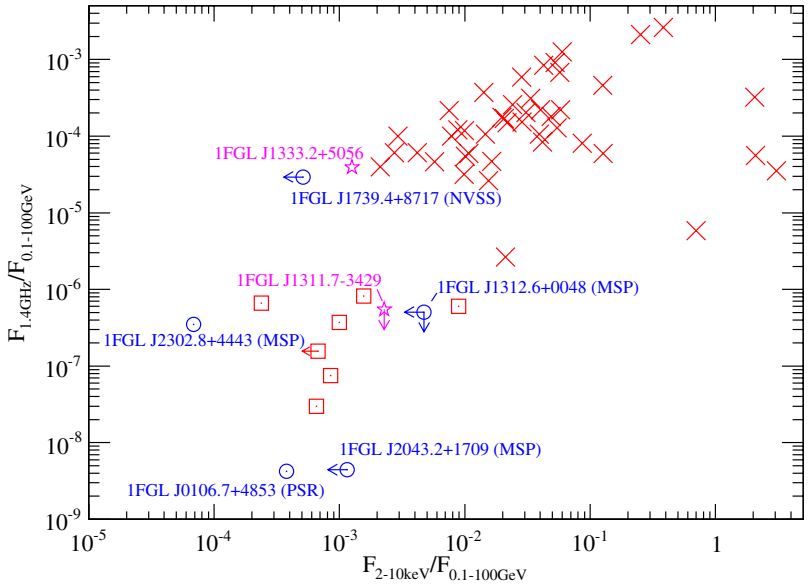

Figure 17. X-ray to γ-ray flux ratios vs. radio to γ-ray flux ratios for unassociated *Fermi*-LAT sources. The blue circles show the flux ratios of unassociated *Fermi*-LAT sources which we observed using the *Suzaku* satellite. The γ-ray flux and the radio upper limits of these sources are taken from values of the 1FGL catalog and the NVSS catalog (Condon et al. 1998), respectively. Red × marks indicate the data plots of blazars listed in Abdo et al. (2010f). Red squares represent the data points of the *Fermi*-LAT sources that are associated with MSPs discovered by Cognard et al. (2011) and Ransom et al. (2011), and three *Fermi*-LAT sources listed in Abdo et al. (2010j) for which the best-fit model of the X-ray spectra were determined. The values of X-ray flux and radio fluxes of MSPs in Abdo et al. (2010j) are quoted and derived from Bailes et al. (1997), Lundgren et al. (1995), Navarro et al. (1995), Sakurai et al. (2001), Webb et al. (2004a), and Webb et al. (2004b). For the MSPs we cannot quote the radio flux at 1.4 GHz, we estimated 1.4 GHz flux by the extrapolation using radio fluxes that are available in the literature assuming a power-law model. Pink stars show the two still unassociated 1FGL sources from our first year campaign targets (Maeda et al. 2011) and another two 1FGL sources studied in Maeda et al. (2011) and that are now associated with MSPs are involved in red squares.

(A color version of this figure is available in the online journal.)

Finally, we comment in more detail on the case of 1FGL J2302.8+4443. This object, as already mentioned above, has recently been associated with the MSP PSR J2302+4442 discovered by the Nançay radio telescope (Cognard et al. 2011). The rotation period of the pulsar is $P \simeq 5.19$ ms, the spin-down luminosity is $\dot{E} \simeq 3.74 \times 10^{33}$ erg s^{-1}, and the characteristic age can be evaluated as $\tau \simeq 6.2$ Gyr. Cognard et al. (2011) also reported on the detection of the X-ray counterpart of the pulsar with *XMM-Newton*, with the unabsorbed 0.5–3 keV flux of $3.1^{+0.4}_{-0.4} \times 10^{-14}$ erg cm^{-2} s^{-1}. This is consistent with our *Suzaku* detection (the re-calculated flux in the same photon energy range $2.9^{+1.1}_{-1.2} \times 10^{-14}$ erg cm^{-2} s^{-1}). Anticipating the distance of the pulsar $d \simeq 1.18$ kpc which was inferred from the NE2001 model of Galactic free electron density (Cordes & Lazio 2001), the X-ray luminosity of PSR J2302+4442 can therefore be evaluated roughly as $L_{\rm x} \sim 3 \times 10^{30}$ erg s^{-1}. This, together with $\dot{E}$ provided above, is then in good agreement with the scaling relation between the X-ray and spin-down luminosities $L_{\rm x} \sim 10^{-3} \times \dot{E}$ established for MSPs (Becker & Truemper 1997; Gaensler & Slane 2006; Zhang et al. 2007), although the inferred distance of PSR J2302+4442 is indicated to be smaller by a factor of four considering an unphysically high γ-ray efficiency and, instead, assuming average efficiency of γ-ray MSPs ~ 10 % (Cognard et al. 2011).

The spectrum of the X-ray counterpart of PSR J2302+4442/1FGL J2302.8+4443 was well fit by a blackbody model, and this is again in agreement with the idea that the observed X-ray photons originate from thermal emission from the surface of a rotating magnetized neutron star. Because of the limited photon statistics in the higher energy range of XIS, we could not however confirm the presence of a non-thermal component above 2 keV (clearly detected in the case of 1FGL J1231.1−1410 by Maeda et al. 2011). Interestingly, for the isolated pulsars as old as PSR J2302+4442 (characteristic age of about 6 Gyr), the surface temperature of the neutron star is expected to be $T \lesssim 10^5$ K (Nomoto & Tsuruta 1987; Page & Applegate 1992). Our detection of the X-ray counterpart indicated $kT \simeq 0.31 \pm 0.03$ keV, i.e., $T \simeq 3.6 \times 10^6$ K instead. Some reheating process is therefore required, possibly related to the impact of relativistic particles on polar caps (Becker & Truemper 1997, and references therein).

C.C.C.'s work at NRL is sponsored by NASA DPR S-15633-Y. Ł.S. is grateful for the support from Polish MNiSW through the grant N-N203-380336. We thank the anonymous referee for a careful reading of the manuscript and useful suggestion which helped to improve the paper.

REFERENCES

Abdo, A. A., Ackermann, M., Agudo, I., et al. 2010a, ApJ, 716, 30
Abdo, A. A., Ackermann, M., Ajello, M., et al. 2009b, ApJS, 183, 46
Abdo, A. A., Ackermann, M., Ajello, M., et al. 2009c, ApJ, 701, L123
Abdo, A. A., Ackermann, M., Ajello, M., et al. 2010d, ApJS, 187, 460
Abdo, A. A., Ackermann, M., Ajello, M., et al. 2010e, ApJS, 188, 405
Abdo, A. A., Ackermann, M., Ajello, M., et al. 2010f, ApJ, 709, L152
Abdo, A. A., Ackermann, M., Ajello, M., et al. 2010g, ApJ, 710, L92
Abdo, A. A., Ackermann, M., Ajello, M., et al. 2010h, ApJ, 714, 927
Abdo, A. A., Ackermann, M., Ajello, M., et al. 2010i, ApJ, 720, 912
Abdo, A. A., Ackermann, M., Ajello, M., et al. 2010j, A&A, 512, A7
Abdo, A. A., Ackermann, M., Ajello, M., et al. 2010k, A&A, 524, A75
Abdo, A. A., Ackermann, M., Ajello, M., et al. 2010l, Science, 325, 848
Abdo, A. A., Ackermann, M., Ajello, M., et al. 2012, ApJS, submitted (arXiv: 1108.1435)
Ackermann, M., Ajello, M., Allafort, A., et al. 2011, ApJ, 743, 171
Akamatsu, H., Hoshino, A., Ishisaki, Y., et al. 2011, PASJ, 63, 1019
Atwood, W. B., Abdo, A. A., Ackermann, M., et al. 2009, ApJ, 697, 1071
Bailes, M., Johnston, S., Bell, J. F., et al. 1997, ApJ, 481, 386
Baldwin, J. E., Boysen, R. C., Hales, S. E. G., et al. 1985, MNRAS, 217, 717
Becker, W., & Truemper, J. 1997, A&A, 326, 682
Burrows, D. N., Hill, J. E., Nousek, J. A., et al. 2005, Space Sci. Rev., 120, 165
Casandjian, J.-M., & Grenier, I. A. 2008, A&A, 489, 849
Cognard, I., Guillemot, L., Johnson, T. J., et al. 2011, ApJ, 732, 47
Condon, J. J., Cotton, W. D., Greisen, E. W., et al. 1998, AJ, 115, 1693
Cordes, J. M., & Lazio, T. J. W. 2001, ApJ, 549, 997
Crawford, F., Roberts, M. S. E., Hessels, J. W. T., et al. 2006, ApJ, 652, 1499
Day, C., Arnaud, K., Ebisawa, et al. 1998, The ASCA Data Reduction Guide, Technical Report (Greenbelt: NASA GSFC), v.2.0
Gaensler, B. M., & Slane, P. O. 2006, ARA&A, 44, 17
Guillemot, L., Freire, P. C. C., Cognard, I., et al. 2012, MNRAS, submitted
Hartman, R. C., Bertsch, D. L., Bloom, S. D., et al. 1999, ApJS, 123, 79
Ishisaki, Y., Maeda, Y., Fujimoto, R., et al. 2007, PASJ, 59, 113
Kaaret, P., & Cottam, J. 1996, ApJ, 462, L35
Kalberla, P. M. W., Burton, W. B., Hartmann, D., et al. 2005, A&A, 440, 775
Kokubun, M., Makishima, K., Takahashi, T., et al. 2007, PASJ, 59, 53
Koyama, K., Tsunemi, H., Dotani, T., et al. 2007, PASJ, 59, 23
Lundgren, S. C., Zepka, A. F., Cordes, J. M., et al. 1995, ApJ, 453, 419
Maeda, K., Kataoka, J., Nakamori, T., et al. 2011, ApJ, 729, 103
Marelli, M., De Luca, A., & Caraveo, P. A. 2011, ApJ, 733, 82
Matsumoto, H., Ueno, M., Bamba, A., et al. 2007, PASJ, 59, 199
Mitsuda, K., Bautz, M., Inoue, H., et al. 2007, PASJ, 59, 1
Monet, D. G., Levine, S. E., Canzian, B., et al. 2003, AJ, 125, 984
Navarro, J., Bruyn, A. G., Frail, D. A., et al. 1995, ApJ, 455, L55
Nomoto, K., & Tsuruta, S. 1987, ApJ, 312, 711
Page, D., & Applegate, J. H. 1992, ApJ, 394, L17
Pletsch, H. J., Guillemot, L., Allen, B., et al. 2011, ApJ, 744, 105
Ransom, S. M., & Pulsar Search Consortium, F. 2010, BAAS, 42, 655
Ransom, S. M., Ray, P. S., Camilo, F., et al. 2011, ApJ, 727, L16
Rengelink, R. B., Tang, Y., de Bruyn, A. G., et al. 1997, A&AS, 124, 259
Romero, G. E., Benaglia, P., & Torres, D. F. 1999, A&A, 348, 868
Roming, P. W. A., Kennedy, T. E., Mason, K. O., et al. 2005, Space Sci. Rev., 120, 95
Sakurai, I., Kawai, N., Torii, K., et al. 2001, PASJ, 53, 535
Skrutskie, M. F., Cutri, R. M., Stiening, R., et al. 2006, AJ, 131, 1163
Sowards-Emmerd, D., Romani, R. W., & Michelson, P. F. 2003, ApJ, 590, 109
Sowards-Emmerd, D., Romani, R. W., Michelson, P. F., Healey, S. E., & Nolan, P. L. 2005, ApJ, 626, 95
Sowards-Emmerd, D., Romani, R. W., Michelson, P. F., & Ulvestad, J. S. 2004, ApJ, 609, 564
Takahashi, T., Abe, K., Endo, M., et al. 2007, PASJ, 59, 35
Thompson, D. J. 2004, in Cosmic Gamma-Ray Sources, Vol. 304, ed. K.S. Cheng (Dordrecht: Kluwer), 149
Thompson, D. J., Bailes, M., Bertsch, D. L., et al. 1999, ApJ, 516, 297
Uchiyama, Y., Maeda, Y., Ebara, M., et al. 2008, PASJ, 60, 35
Webb, N. A., Olive, J.-F., & Barret, D. 2004a, A&A, 417, 181
Webb, N. A., Olive, J.-F., Barret, D., et al. 2004b, A&A, 419, 269
Yadigaroglu, I.-A., & Romani, R. W. 1997, ApJ, 476, 347
Zhang, L., Fang, J., & Chen, S. B. 2007, ApJ, 666, 1165